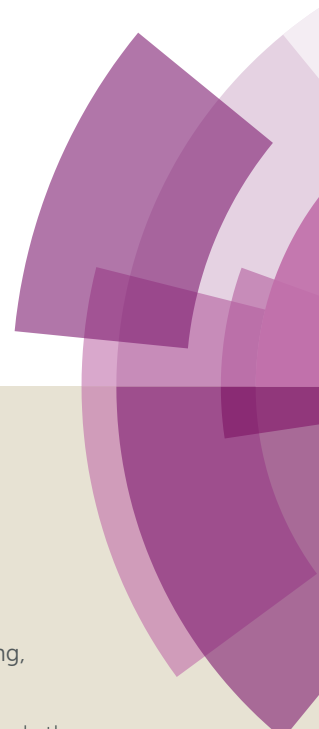


Dalton Transactions

Accepted Manuscript



This article can be cited before page numbers have been issued, to do this please use: D. Wu, W. Huang, F. Pan, Z. Wang, Z. Ouyang, X. Feng, J. Gu and Y. Bai, *Dalton Trans.*, 2017, DOI: 10.1039/C7DT00564D.



This is an Accepted Manuscript, which has been through the Royal Society of Chemistry peer review process and has been accepted for publication.

Accepted Manuscripts are published online shortly after acceptance, before technical editing, formatting and proof reading. Using this free service, authors can make their results available to the community, in citable form, before we publish the edited article. We will replace this Accepted Manuscript with the edited and formatted Advance Article as soon as it is available.

You can find more information about Accepted Manuscripts in the [author guidelines](#).

Please note that technical editing may introduce minor changes to the text and/or graphics, which may alter content. The journal's standard [Terms & Conditions](#) and the ethical guidelines, outlined in our [author and reviewer resource centre](#), still apply. In no event shall the Royal Society of Chemistry be held responsible for any errors or omissions in this Accepted Manuscript or any consequences arising from the use of any information it contains.



Journal Name

Mixed-Valence Metallogrid [Co^{III}₂Co^{II}₂] with Unusual Electronic Structure and Single-Ion-Magnet Characterization

Received 00th January 20xx,
Accepted 00th January 20xxWei Huang,^a Feifei Pan,^a Zhenxing Wang,^b Yan Bai,^c Xuejun Feng,^{*a} Jiande Gu,^a Zhong-Wen Ouyang^b and Dayu Wu^{*a}

DOI: 10.1039/x0xx00000x

www.rsc.org/

The reaction of the multisite coordination ligand (**H₂L**) with Co(Ac)₂ · 4H₂O in the absence of any base affords a homometallic tetranuclear mixed-valence complex, [Co₄(L)₄(CH₃CO₂)₂(CH₃OH)₂]·Et₂O (**1**). The mixed-valence metallogrid [Co₄(L)₄(CH₃CO₂)₂(CH₃OH)₂]·Et₂O (**1**) has been theoretically and experimentally analyzed to assign the valence and spin state in the form of *trans*-[Co^{III}_{1s}-Co^{II}_{1hs}-Co^{III}_{1s}-Co^{II}_{1hs}]. HF-EPR reveals the presence of axial anisotropy ($D = -34.4 \text{ cm}^{-1}$) with a significant transverse component ($E = 9.5 \text{ cm}^{-1}$) for the local high spin cobalt centers. Slow magnetic relaxation effects were observed in the presence of a dc field, demonstrating field-induced single ion magnet behavior, which is associated with the unusual electronic structure of Co(II) within the metallogrid.

Introduction

The transition-metal mononuclear complexes rather than polynuclear aggregates have shown promise as single-molecule-magnet (SMM) candidates.¹ For transition-metal clusters, the height of the energy barrier and therefore the SMM behavior depends on the large-spin multiplicity of the ground state (S_T) and the Ising-type magnetic anisotropy of the molecule ($D < 0$).² However, slow magnetic relaxation for mononuclear first-row transition metal complexes was frequently prohibited because fast quantum tunneling magnetization (QTM) may prevent the magnetization relaxation through a thermally activated mechanism, and in most cases it is effective to exert a small magnetic field to suppress tunnelling and induce the slow magnetization relaxation (so-called field-induced single-ion magnet).^{3,4} It is believed that the low coordination environment of first-row transition metal complexes forms a relatively weak ligand field, resulting in the d orbital energy splitting with a small separation between the electronic ground state and the excited states, thus maximizing the spin-orbit coupling to enhance the magnetic anisotropy.⁵⁻⁷ Indeed, variation of

the ligand donor characteristics can then provide a means of tuning the magnetic anisotropy despite of positive or negative sign.⁸

Previously, we reported the trinuclear linear Co^{III}-Co^{II}-Co^{III} mixed-valence single-molecule magnets.⁹ Magnetic analyses revealed that central Co(II) was magnetically isolated by two terminal diamagnetic Co(III) subunits, in which the energy scale of anisotropy may stem from the transverse zero-field splitting. Here, we employed the multi-site coordination donor to self-assemble the tetranuclear mixed-valence cobalt complex, [Co₄(L)₄(CH₃CO₂)₂(CH₃OH)₂]·Et₂O (**1**), in the form of Co^{III}-Co^{II}-Co^{III}-Co^{II} valence alignment, in which L is a doubly deprotonated multidentate ligand as depicted in Scheme 1. Complex **1** contains two magnetically-isolated weakly coordinated octahedral Co(II) ions with axial anisotropy and large transverse component. Slow relaxation of the magnetization that is characteristic of Single-Molecule Magnet (SMM) behavior was observed.

Experimental Section

Reagents and General Procedures

All of the reagents employed were commercially available and were used without further purification. Perdeuterated dimethyl sulfoxide (DMSO-*d*⁶) was purchased from Alfa Aesar Co. Ltd. Elemental analyses (C, H, and N) were conducted with a PerkinElmer 2400 analyzer. Micro-IR spectroscopy studies were performed on a Nicolet Magna-IR 750 spectrophotometer in the 4000–400 cm⁻¹ region (w, weak; b, broad; m, medium; s, strong) by a KBr disk. ¹H NMR spectra were obtained from a solution in deuterated DMSO using a Bruker-400 spectrometer (s, singlet; d, doublet; t, triplet; m, multiplet; dd, double doublet).

Synthetic route of ligand **H₂L** is shown in Scheme 1. 2-oxoquinoline-3-carbaldehyde was prepared according to the literature method.¹⁰ A mixture ethanolic solution (80mL) of benzoyl hydrazine

^aJiangsu Key Laboratory of Advanced Catalytic Materials and Technology, Collaborative Innovation Center of Advanced Catalysis & Green Manufacturing, School of Petrochemical Engineering, Changzhou University, Changzhou, Jiangsu 213164, China; E-mail: wudy@cczu.edu.cn; fengxuejun@cczu.edu.cn

^bWuhan National High Magnetic Field Center, Huazhong University of Science and Technology, 430074 Wuhan, China

^cKey Laboratory of Polyoxometalate Chemistry of Henan Province, School of Chemistry and Chemical Engineering, Henan University, Kaifeng, 475004, People's Republic of China

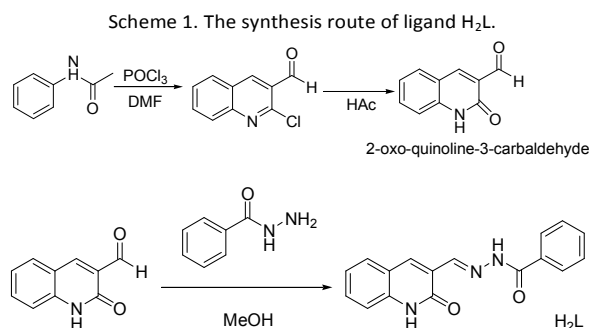
†Electronic Supplementary Information (ESI) available: Additional magnetic, structural, and spectroscopic characterization data. This material is available free of charge via the Internet at <http://pubs.acs.org>. For ESI and crystallographic data in CIF or other electronic format see DOI: 10.1039/x0xx00000x

ARTICLE

Journal Name

(10mmol, 1.36g) and 2-oxo-quinoline-3-carbaldehyde (10mmol, 1.73 g) was refluxed for 2 h under nitrogen atmosphere; after it was cooled to room temperature, a pale yellow solid was obtained by filtration under reduced pressure. The crude product was washed with cold ethanol and dried in vacuo. Yield: 86%. $^1\text{H NMR}$ (in $\text{DMSO-}d^6$): δ 8.73(s, 1H), 8.49(s, 1H), 7.96(t, 2H), 7.87(t, 1H), 7.61(m, 1H), 7.55(m, 4H), 7.46(t, 1H), 7.36(d, 1H), 7.23(t, 1H). Elemental analysis for $\text{C}_{17}\text{H}_{13}\text{O}_2\text{N}_3$. Calculated: H, 4.50; C, 70.09; N, 14.42. Found: H, 4.75; C, 69.38; N, 14.67%.

Preparation of compound 1. A solution of $\text{Co}(\text{OAc})_2 \cdot 4\text{H}_2\text{O}$ (0.10mmol, 0.025g) in methanol (10ml) was added to a methanol solution of ligand H_2L (0.1mmol, 0.029g) in the absence of any base, the mixture solution was stirred for another 15 min. The suspension was then filtered, and the filtrate was diffused with diethyl ether. Dark-red block-shaped single crystals suitable for X-ray diffraction analysis were obtained after several days. Yield: 68%. IR(KBr pellet, cm^{-1}): 3404(s), 1613(s), 1590(w), 1562(w), 1508(m), 1494(m), 1438(w), 1381(w), 1185(m), 781(w), 754(w), 702(w), 668(w). Anal. Calcd for $\text{C}_{78}\text{H}_{68}\text{Co}_4\text{N}_{12}\text{O}_{15}$: H, 4.16; C, 56.81; N, 10.19. Found: H, 4.43; C, 57.05; N, 10.65.



Single-Crystal Structure Determination

The diffraction intensity data of complex **1** at 120(2) K were collected on a Bruker APEX-II CCD with graphite-monochromated $\text{Mo K}\alpha$ radiation ($\lambda = 0.71073 \text{ \AA}$). Data collection, data reduction, and cell refinement were performed by using the Bruker Instrument Service v4.2.2 and SAINT V8.34A software.^{11,12} Structures were solved by direct methods using the SHELXS program, and refinement was performed using SHELXL based on F^2 through full-matrix least-squares routine.¹³ Absorption corrections were applied upon using multiscan program SADABS.¹⁴ Hydrogen atoms of organic ligands were generated geometrically by the riding mode, and all the non-hydrogen atoms were refined anisotropically through full-matrix least-squares technique on F^2 with the SHELXTL program package.^{15,16} A summary of the crystallographic data and refinement parameters is shown in Table 1. Selected bond lengths and bond angles for **1** are listed in Table S1.

Magnetic Measurement

Variable-temperature (2.0–300 K) direct current (dc) magnetic susceptibility measurements under an applied field of 1.0 kG, and

variable-field (0–5.0 T) magnetization measurements at low temperatures in the range of 2.0–10.0 K were carried out with a Quantum Design SQUID magnetometer. Alternating current (ac) susceptibility measurements were performed under an oscillating field of 3 Oe and ac frequencies in the range from 1 to 1500 Hz. The magnetic data were corrected for the sample holder and the intrinsic diamagnetic contributions from Pascal constants.¹⁷ Dc and ac magnetic measurements were carried out by restraining the sample in eicosane in order to prevent any torquing due to its magnetic anisotropy.

HF-EPR

HF-EPR measurements were performed on a locally developed spectrometer at the Wuhan National High Magnetic Field Center, using a pulsed magnetic field of up to 30 T.^{18,19}

Theoretical Investigation

Gaussian 09 was used for all the computations and the Minnesota density functional M06-L and M06-2x and the valence double zeta basis set, augmented with d -type polarization functions as well as the diffuse functions for heavy elements and p -type polarization functions for H, namely 6-31+G(d,p) were employed.

In the model complex, the doubly deprotonated multidentate ligand (L in the complex) was simplified by eliminating the phenyl groups at the terminal of the ligand. (Fig. S2, ESI).

Mulliken spin density values of main atoms, the total energy (in Hartree) and the cartesian coordinates for the optimised structure of the complex are provided in the supporting materials. (ESI, Table S2-3) The optimized geometry of the modeled complex is depicted in supporting materials, Fig. S3, in which the N–Co(II) atomic distances amount 2.06 to 2.09 Å and the O–Co(II) distances varies from 1.98 to 2.23 Å. These values are close to those observed in the crystal measurements. The model adopted in the DFT study reasonably represents the complex **1**. MO analysis reveals that the d_z^2 and $d_{x^2-y^2}$ of Co(III) are unoccupied in the complex (Fig. S4).

Table 1. Summary of crystallographic data for **1**.

Empirical formula	$\text{C}_{78}\text{H}_{68}\text{Co}_4\text{N}_{12}\text{O}_{15}$	
Formula weight	1649.16	
Crystal system	Triclinic	
Space group	$P-1$	
a (Å)	14.9882(11)	
b (Å)	15.0573(12)	
c (Å)	17.6800(13)	
α (°)	74.232(2)	
β (°)	82.418(2)	
γ (°)	66.125(2)	
V (Å ³)	3510.2(5)	
Z	2	
$F(000)$	1696	
Goodness-of-fit on F^2	1.077	
R_1, wR_2 ($I > 2\sigma(I)$) ^a	0.0614	0.1805
R_1, wR_2 (all data) ^a	0.0898	0.2443
Residuals (e Å ⁻³)	1.041, -1.067	

^a $R_1 = \sum ||F_o| - |F_c|| / \sum |F_o|$; $wR_2 = [\sum [w(F_o^2 - F_c^2)^2] / \sum [w(F_o^2)^2]]^{1/2}$. ^bGOF = $[\sum [w(F_o^2 - F_c^2)^2] / (N_{\text{obs}} - N_{\text{params}})]^{1/2}$, based on the data $I > 2\sigma(I)$.

Results and Discussion

X-ray Structure Analysis

The crystal structure of complex **1** contains neutral tetranuclear $[\text{Co}_4(\text{L})_4(\text{CH}_3\text{CO}_2)_2(\text{CH}_3\text{OH})_2]$ unit in addition to an ether molecule as shown in Fig. 1.²⁰ Within the individual ligand, the C–N bond distances of 1.336(3), 1.365(7) and 1.317(7) Å for C7–N1, C16–N3 and C17–N3 bonds, respectively, are the intermediate between the normal single bond and double one, suggesting that the protons on all the carbohydrozone and imine groups get lost and L acts as a dianionic ligand in the complex (denoted as L). Two corner cobalt atoms Co1 and Co3, with the separation of 5.995 Å, are octahedrally coordinated to two chelating ligands and form CoN_2O_4 coordination sphere with the comparable Co–O and Co–N bond distance varying from 1.856(4) to 1.917(4) Å, the bite angle in the two ligands is very close to 90° , and the full set of angles about Co1 range between 83.2° and 93.3° , while another pair of corner cobalt atoms, Co(2) or Co(4), are separated by 6.125 Å and each one is located around the heavily distorted octahedral sphere by two monodentate N atoms from two different ligands, one methanol molecule and one acetate anion with M–L distance of ca. 2.0 Å. In addition, two weakly coordination sites exist around Co4 with Co4...O2 separation being 2.601 Å and Co4...O8 (2.578 Å). The octahedral coordination about Co4 is severely distorted with the bite angle O2–Co–N3 and O8–Co4–N12 of ca. 55° . The similar coordination sphere is found on its diagonal Co2, and the weak coordination is evidenced by Co2...O4 contact of 2.355 Å and Co2...O5 of 2.544 Å. As expected, the low-spin Co^{3+} ions allow the ligand donor atoms to be significantly shorter (~ 0.2 Å) than the analogous distances involving the high-spin Co^{2+} ions. The bond distances around the Co(2) and Co(4) center are obviously longer than those of Co(1) and Co(3); two Co–N bond distances vary between 2.028(5) and 2.044(4) Å and Co–O distances range from 1.981(4) to 2.065(4) Å with the exceptionally long Co...O weak coordination, all of which are indicative of high-spin Co^{2+} ($S = 3/2$) for Co(2)/Co(4) and low-spin Co^{3+} ($S = 0$) for Co(1)/Co(3), respectively. The oxidation state of four cobalt ions was assigned on the basis of these bond length considerations, charge balance, and BVS calculations. BVS values of 4.49, 2.27, 4.48 and 2.28 for the Co(1), Co(2), Co(3) and Co(4) centers, respectively, support the valence assignment on the basis of bond lengths.²¹ The analysis of X-ray diffraction data can give rise to a mixed-valence metallogrid complex of the $\text{Co}^{\text{III}}\text{--Co}^{\text{II}}\text{--Co}^{\text{III}}\text{--Co}^{\text{II}}$ form. The UV-vis-NIR spectra was further checked to show no inter-valence charge transfer band (IVCT). (Fig. S5, ESI) Hence, the compound **1** is a valence-localized (type-I) mixed valence system without electronic interactions between Co(II) and Co(III).

To further confirm the X-ray diffraction results on assigning the valence and spin state, the density functional theory (DFT) calculations were used to optimize the geometries and electronic structure using the Gaussian 09 code.^{22–25} The total spin density of the model system as depicted in Fig. 1(c) clearly indicates that the spin density of the system is largely limited on the two high-spin cobalt ions.²⁶ The successive molecular orbital (MO) analysis demonstrates that three singly occupied MOs (SMO) are well-

localized on the d orbitals (d_{xy} , $d_{x^2-y^2}$, and d_{z^2}) for each high-spin Co(II) ion. (Fig. 1(d)) It should be noted that the spin-spin interaction between Co(II) ions can be ignored. The DFT calculations of the open-shell singlet state of this model complex results in the same total energy as compared to that based on the septet state calculations.

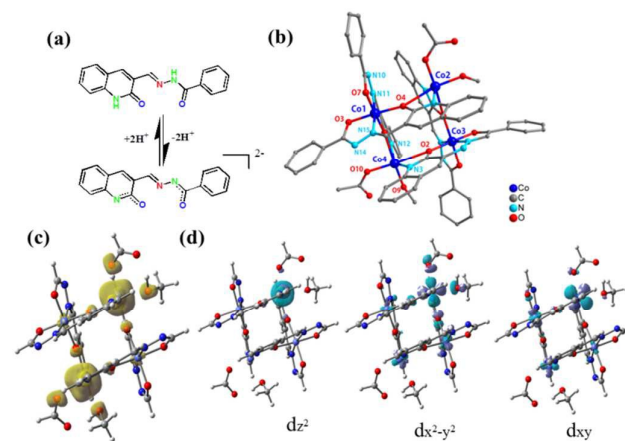


Fig. 1. (a) Ligand structure and its deprotonation formation upon metal coordination. (b) Crystal structure of the complex **1** with the selected atom scheme and the solvent molecule omitted for clarity. (c) The total spin density of the model complex. (d) The singly-occupied molecular orbitals (SMOs) localized on Co(2). Similar SMOs on Co(4) are not displayed here for clarity.

Magnetic Study

Temperature- and field-dependent magnetic data are depicted in Fig. 2, where χ_M is the molar magnetic susceptibility per $\text{Co}^{\text{III}}_2\text{Co}^{\text{II}}_2$ unit. The $\chi_M T$ value of $5.15 \text{ emu K mol}^{-1}$ at room temperature corresponds to the value expected for two $S = 3/2$ ions with $g = 2.34$. These values substantially exceed the spin-only value for two high-spin cobalt(II) ions ($S = 3/2$, $1.875 \text{ cm}^3 \text{ mol}^{-1} \text{ K}$ with $g = 2$). This is indicative of an unquenched orbital contribution of the Co^{2+} ion in a distorted-octahedral geometry. When the temperature is further lowered, the $\chi_M T$ decreases pronounced to reach the values of $3.52 \text{ cm}^3 \text{ mol}^{-1} \text{ K}$ at 2 K. This behavior is due to the local anisotropy of the Co^{2+} ion promoted by the spin-orbit coupling (SOC) rather than intramolecular interactions between paramagnetic Co(II) ions through the diamagnetic Co^{III} linkage. The data could be analyzed through a Hamiltonian for mononuclear model that takes into account spin-orbit coupling, axial distortion of the octahedral geometry, and Zeeman interactions.²⁷

$$\mathbf{H} = -\frac{3}{2}\kappa\lambda LS + \Delta(L_z^2 - 2/3) + \beta[-\frac{3}{2}\kappa L + g_e S]H \quad (1)$$

where κ is the orbital reduction factor, λ is the spin-orbit coupling parameter, and Δ is the axial orbital splitting of the ${}^4\text{T}_{1g}$ term. The factor $-3/2$ comes from the fact that the real angular momentum for the ${}^4\text{T}_{1g}$ ground state in an ideal O_h geometry is equal to the angular momentum of the ${}^4\text{P}$ free ion term multiplied by $-3/2$. The best-fit parameters were as following: $\kappa = 0.79$, $\lambda = -57$, $\Delta = 351 \text{ cm}^{-1}$, $R = 6 \times 10^{-5}$. The fitting parameters are in good accordance with previously reported values for distorted-

ARTICLE

Journal Name

octahedral Co(II) complexes and indicate the distortion from the ideal octahedral configuration.²⁸

To further determine the magnitude and sign of the anisotropy parameter, we determined the field dependence of the magnetization of complex **1** at fields ranging from 0.05 to 5 T between 2 and 10 K (inset, Fig. 2). The M vs H/T plots for **1** are not superimposed on a single master curve, clearly indicating the presence of a significant magnetic anisotropy. The magnetization of the sample at 5 T and 2 K is $M = 4 \mu_B$, which is far below the expected saturation value for two $S = 3/2$ and $g = 2.34$ ($M_{\text{sat}} = 7.0 \mu_B$) and is another indication of large ZFS. Indeed, the low-temperature experimental magnetization data were then analyzed using ANISOFIT version 2.0, which takes into account the axial (D) and transverse (E) magnetic anisotropies in the spin Hamiltonian²⁹:

$$\hat{H} = D\hat{S}_z^2 + E(\hat{S}_x^2 - \hat{S}_y^2) + g\mu_B\hat{S}H \quad (2)$$

where S is the spin ground state, g is the average g factor, μ_B is the Bohr magneton, and H is the magnetic field. The best-fit values of the parameters were as follows: $D = -34.8(5) \text{ cm}^{-1}$, $E = 6.7(6) \text{ cm}^{-1}$, and $g = 2.5(2)$ with $f = 0.0010$ (solid lines in Fig. 2, inset). Optimization by setting the initial D to a positive value does not converge to a reliable fit, indicating the correct choice of the sign. Because D is negative, the $M_s = \pm 3/2$ Kramers doublet is below the $M_s = \pm 1/2$ Kramers doublet.

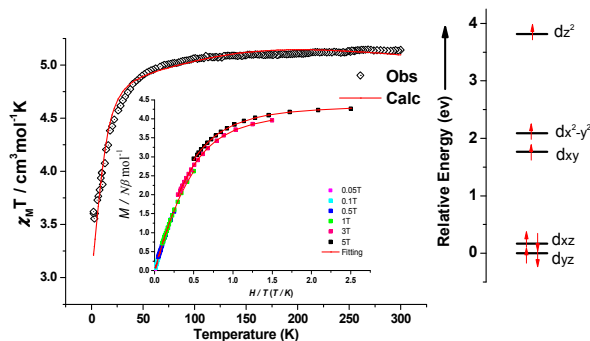


Fig. 2 (Left) Temperature dependence of χ_M'' for complex **1** under the magnetic field of 0.25 T. Solid lines represent the calculated result with the Hamiltonian of eq 1. Inset is low-temperature magnetization data for **1** collected in the temperature range of 2–10 K under various applied dc fields of 0.05–5 T. Solid red lines correspond to best fits obtained with ANISOFIT 2.0.¹⁹ (Right) Removal of the degeneracy of the d orbitals on Co2 and Co4 and their relative energy level diagrams of d orbitals.

The large and negative zero-field splitting D parameter for compound **1** indicate the existence of an important axial anisotropy and therefore the possibility of slow magnetic relaxation. Under a zero dc field, no maximum in the out-of-phase ac susceptibility signal (χ_M'') of both the frequency and temperature dependent plots was observed for **1** (Fig. S7, ESI[†]), which is due to very fast quantum tunnelling of magnetization (QTM). Although no peaks of χ_M'' are observed under zero dc magnetic field, non-zero χ_M'' signals appeared under an applied field of 1.0 kG (this field was chosen because it induces slower relaxation (Fig. S7 and Table S4, ESI), indicating a slowly relaxing magnetic moment. To obtain quantitative information regarding the spin relaxation barrier, the frequency dependence of χ_M'' and χ_M' at the different temperatures

was examined as shown in Fig. 3(a) (Fig. S8, SI). Debye model was used to extract relaxation times (τ) at different temperatures. The results were employed in constructing the Arrhenius plots [$\tau = \tau_0 \exp(U_{\text{eff}}/k_B T)$] shown as inset of Fig. 3b. Assuming a thermally activated mechanism, a fit to the linear data would provide the activation energy ($U_{\text{eff}} = 17.7 \text{ cm}^{-1}$) and the pre-exponential factor ($\tau_0 = 5.5 \times 10^{-8} \text{ s}$). Obviously, U_{eff} is much smaller than the zero-field energy gap of magnitude $2D$ as predicted by the static magnetic measurements. This means that the derived energy barrier cannot be correct. Similar observations have recently been reported for other mononuclear cobalt complex.^{8f}

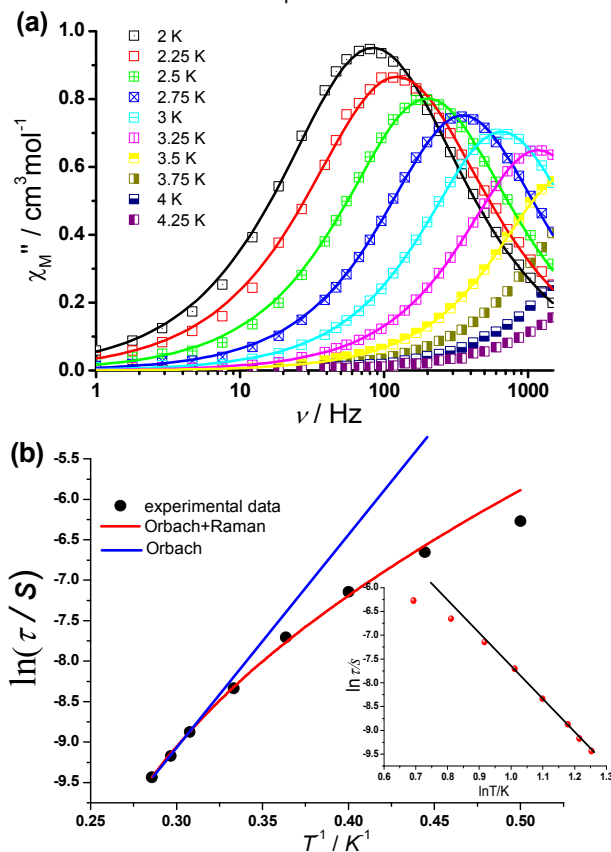


Fig. 3 (a) Frequency dependence of out-of-phase (χ_M'') ac susceptibilities for **1** under 1000 Oe dc field. The solid lines are the best fitting to the generalized Debye model. (b) Natural logarithm of the relaxation time $\ln \tau$ vs T^{-1} . The curved red line is the fit to sum of Raman and Orbach processes with $U_{\text{eff}} = 68.8 \text{ cm}^{-1}$ (fixed). Inset is power law for **1** between 2.0 K and 3.5 K.

The Cole–Cole plots for compound **1** at different temperatures under a 1.0 kG dc field also display signatures of slow magnetic relaxation (Fig. 4). The Cole–Cole diagrams in the temperature range 2–4.25 K for **1** exhibit semicircular shapes. The fit of the χ_M'' vs χ_M' data at each temperature using the generalized Debye mode (see equation S1 in the Supporting Information) yielded the values of χ_T (isothermal susceptibility), χ_S (adiabatic susceptibility), and α (this parameter determines the width of the distribution of relaxation times, so that $\alpha = 1$ corresponds to an infinitely wide distribution of relaxation times, whereas $\alpha = 0$ represents a

relaxation with a single time constant). Fitting the data gives the calculated values of α within the relatively wide range of 0.002–0.2 at the different temperatures (Table S5, Supporting Information), which is indicative of multiple relaxation processes and the presence of a non-negligible remaining QTM relaxation.

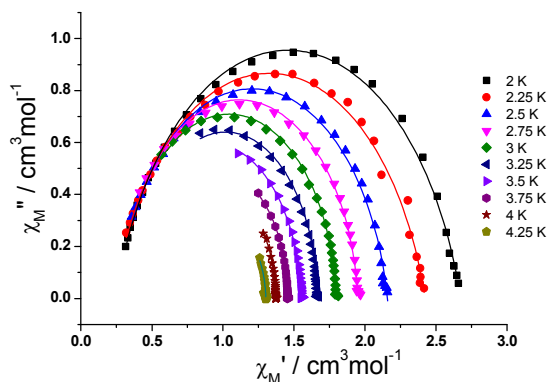


Fig. 4. Cole–Cole plot of χ_M'' vs χ_M' over the temperature range of 2.0–4.25 K under a 1000 Oe applied dc field for compound **1**. The solid line represents a least-squares fitting of the data using the generalized Debye mode.

To resolve this discrepancy, we recorded high-field, high-frequency electron paramagnetic resonance (HF-EPR) spectra at different frequencies and up to an applied magnetic field of 10 T of complex **1** to confirm the magnetization results, and specifically the negative sign of D parameters (Fig. 5). The low-temperature powder data are typical for an anisotropic system described by the zero-field Hamiltonian $H = DS_z^2 + E(S_x^2 - S_y^2) + g\mu_B S_H$. Here, three components are observed for complex **1**, corresponding to transitions between two Kramers doublets ($m_s = \pm 1/2$ and $\pm 3/2$) according to the selection rule $\Delta m_s = \pm 1$, with one low field component [effective Landé constant $g_{x,\text{eff}} = 6.66(7)$ for **1** separated from two high-field components [$g_{y,\text{eff}} = 2.62(8)$ and $g_{z,\text{eff}} = 1.65(8)$]. This pattern of g values is characteristic of an orbitally nondegenerate ground state with a negative D value. To precisely determine the axial D and transverse E terms, spectral simulations were performed under the Hamiltonian mentioned above when considering spin ground state anisotropy. Assuming uniaxial anisotropy D is close to that evaluated from M versus H/T analysis, a good simulation of the spectra can be achieved as shown in Fig. 5b by setting the anisotropic g tensor.³⁰ The parameters are as follows: $g_x = g_y = 2.58(5)$, $g_z = 2.30(5)$, $D = -34.4(6) \text{ cm}^{-1}$, and $E = 9.5(5) \text{ cm}^{-1}$. This is a clear evidence that the D value is in agreement with the result of magnetization data because an alternative simulation with the same absolute positive D value yields an even larger discrepancy.³¹ We have also tried to neglect the E parameter from the spin Hamiltonian, however, the simulation results are very poor, and no better results are obtained by allowing for an isotropic g tensor.

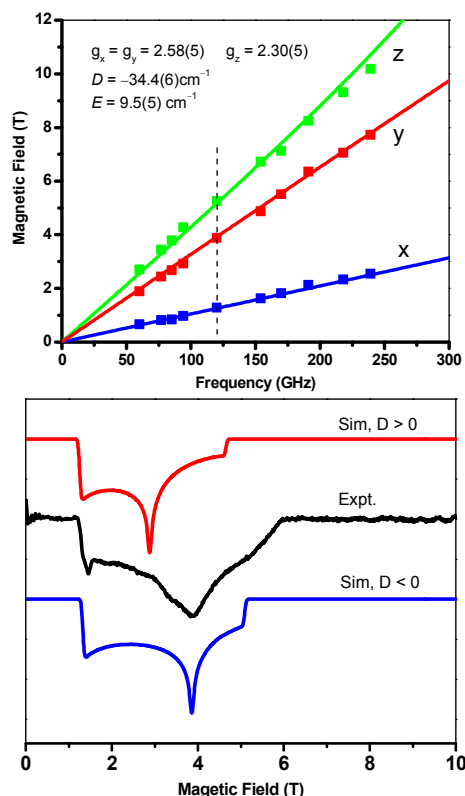


Fig. 5 (a) Frequency dependence of the high-frequency EPR peak positions deduced from studies of a powder sample of **1** at 4.2 K. (b) The best simulation and experimental spectra of 120 GHz in derivative mode at 4.2 K.

The observation of field-induced slow magnetization relaxation in **1** is difficult to understand. Another mononuclear Co^{II} complex with $D < 0$ has been reported recently,^{8f} the quantum relaxation processes are hindering the observation of the full barrier. However, in the case of **1** this explanation does not seem to be pertinent, since quantum tunneling relaxation only contributes in the zero field. Instead, Raman relaxation prevails at most temperatures, and the exponential Orbach pathway becomes important at the highest temperatures only. Nevertheless, the Raman process still influences greatly the overall relaxation properties, so the observed barrier of magnetization reversal ($U_{\text{eff}} = 17.7 \text{ cm}^{-1}$) is far lower than the barrier of Orbach process only ($U = 68.8 \text{ cm}^{-1}$). With the fixed zero-field energy, we revisit the analysis of the ac susceptibility data by considering the additional relaxation process. We have fitted the data in Fig. 3b as a sum of the Orbach and Raman processes with the equation $\tau^{-1} = C\tau^n + \tau_0^{-1} \exp(-U_{\text{eff}}/k_B T)$, keeping the effective energy barrier fixed at $U_{\text{eff}} = 68.8 \text{ cm}^{-1}$. The best fit is obtained for $C = 2.6 \pm 0.3$, $n = 6.7 \pm 0.3$, and $\tau_0^{-1} = 1.8 \times 10^{15} \text{ s}^{-1}$ for **1**. We found that the relaxation times obey a power law ($\tau \sim T^{-n}$; $n = 6.9 \pm 0.1$) in the 2.0–3.5 K temperature range (Fig. 3b, inset), which is indicative that compound **1** involves a dominant Raman processes.^{8h}

Conclusions

In conclusion, we reported the syntheses, structures, and magnetic properties of a new $\text{Co}^{\text{III}}_2\text{Co}^{\text{II}}_2$ tetranuclear mixed-valence complex with general formula $[\text{Co}_4(\text{L})_4(\text{CH}_3\text{CO}_2)_2(\text{CH}_3\text{OH})_2] \cdot \text{Et}_2\text{O}$ (**1**). The

ARTICLE

Journal Name

electronic structures of four cobalt ions were experimentally and theoretically analyzed. DFT calculations provide a direct assignment of the spin distribution. Although both magnetism and HF-EPR revealed compound **1** has significant uniaxial anisotropy D value, they do not exhibit slow relaxation of the magnetization at zero magnetic field. This somewhat surprising behavior is due to the fast quantum tunneling of the magnetization (QTM), the dominant relaxation pathway at zero field. However, under a small magnetic field, the QTM relaxation pathway is suppressed, the relaxation of the magnetization is slowed down, and compound **1** show slow magnetism relaxation behavior. Through control of redox property of transition metal centers, complex **1** is also a promising building block for larger strongly exchange coupled clusters to suppress quantum tunneling.

ACKNOWLEDGMENT

We are thankful for financial support by the Priority Academic Program Development of Jiangsu Higher Education Institutions. This experimental work was financially supported by the National Natural Science Foundation of China (Grants 21471023 & 21671027), Jiangsu Provincial QingLan Project, and Jiangsu Province Key Laboratory of Fine Petrochemical Engineering (KF1302).

Notes and references

- (1) D. Gatteschi, R. Sessoli and J. Villain, *Molecular Nanomagnets*, Oxford University Press: Oxford, U.K., 2006.
- (2) R. Sessoli, D. Gatteschi, A. Caneschi and M. A. Novak, *Nature*, 1993, **365**, 141-143.
- (3) G. Aromi, E. K. Brechin and R. Winpenny, *Springer-Verlag*, 2006, **122**, 1-67.
- (4) S. Gomez-Coca, E. Cremades, N. Aliaga-Alcalde and E. Ruiz, *J. Am. Chem. Soc.*, 2013, **135**, 7010-7018.
- (5) S. Gomez-Coca, D. Aravena, R. Morales and E. Ruiz *Coord. Chem. Rev.*, 2015, **289**, 379-392.
- (6) (a) M. Murrie. *Chem. Soc. Rev.*, 2010, **39**, 1986-1995. (b) J. M. Frost, K. L. M. Harriman and M. Murugesu *Chem. Sci.*, 2016, **7**, 2470-2491. (c) G. A. Craig and M. Murrie *Chem. Soc. Rev.*, 2015, **44**, 2135-2147. (d) S. Vaidya, A. Upadhyay, S. K. Singh, T. Gupta, S. Tewary, S. K. Langley, J. P. S. Walsh, K. S. Murray, G. Rajaraman and M. Shanmugam, *Chem. Commu.*, 2015, **51**, 3739-3742.
- (7) F. Habib, O. R. Luca, V. Vieru, M. Shiddiq, I. Korobkov, S. I. Gorelsky, M. K. Takase, L. F. Chibotaru, S. Hill, R. H. Crabtree and M. Murugesu, *Angew. Chem., Int. Ed.*, 2013, **52**, 11290-11293.
- (8) (a) J. Vallejo, I. Castro, R. Ruiz-García, J. Cano, M. Julve, F. Lloret, G. D. Munno, W. Wernsdorfer and E. J. Pardo, *J. Am. Chem. Soc.*, 2012, **134**, 15704-15707. (b) J. M. Zadrozny, J. Liu, N. A. Piro, C. J. Chang, S. Hill and J. R. Long, *Chem. Commu.*, 2012, **48**, 3927-3929. (c) E. Colacio, J. Ruiz, E. Ruiz, E. Cremades, J. Krzystek, S. Carretta, J. Cano, T. Guidi, W. Wernsdorfer and E. K. Brechin, *Angew. Chem., Int. Ed.*, 2013, **52**, 9130-9134.
- (d) R. Herchel, L. Vahovska, I. Potocnak and Z. Travnicek, *Inorg. Chem.*, 2014, **53**, 5896-5898. (e) T. Jurca, A. Farghal, P. H. Lin, I. Korobkov, M. Murugesu and D. S. Richeson, *J. Am. Chem. Soc.*, 2011, **133**, 15814-15817. (f) J. M. Zadrozny and J. R. Long, *J. Am. Chem. Soc.*, 2011, **133**, 20732-20734. (g) V. V. Novikov, A. A. Pavlov, Y. V. Nelyubina, M. E. Boulon, O. A. Varzatskii, Y. Z. Voloshin and R. E. P. Winpenny, *J. Am. Chem. Soc.*, 2015, **137**, 9792-9795. (h) Y. Rechkemmer, F. D. Breitgoff, M. vander Meer, M. Atanasov, M. Hakl, M. Orlita, P. Neugebauer, F. Neese, B. Sarkar and J. van Slageren, *Nature Commu.*, 2016, **7**, 1-8. (i) R. Ruamps, L. J. Batchelor, R. Guillot, G. Zakhia, A. L. Barra, W. Wernsdorfer, N. Guihéry and T. Mallah, *Chem. Sci.*, 2014, **5**, 3418-3424.
- (9) D. Wu, X. Zhang, P. Huang, W. Huang, M. Ruan and Z. W. Ouyang, *Inorg. Chem.*, 2013, **52**, 10976-10982.
- (10) M. K. Singh, A. Chandra, B. Singh and R. M. Singh, *Tetrahedron Lett.*, 2007, **48**, 5987-5990.
- (11) Bruker SAINT, v8.34A; Bruker AXS Inc: Madison, WI, 2013.
- (12) Bruker APEX2, v2014.5-0; Bruker AXS Inc: Madison, WI, 2007.
- (13) G. M. Sheldrick, *Acta Crystallogr., Sect. A: Found. Crystallogr.*, 2008, **A64**, 112-122.
- (14) Bruker SADABS, Bruker AXS Inc: Madison, WI, 2014.
- (15) SHELXTL V5.1, Software Reference Manual; Bruker, AXS, Inc: Madison, WI, 1997.
- (16) A. L. J. Spek, *Appl. Crystallogr.*, 2003, **36**, 7-13.
- (17) O. Kahn, *Molecular Magnetism*, VCH Publishers, Inc: New York, 1993, p2.
- (18) S. L. Wang, L. Li, Z. W. Ouyang, Z. C. Xia, N. M. Xia, T. Peng and K. B. Zhang, *Acta Phys. Sin.*, 2012, **61**, 107601-107601.
- (19) H. Nojiri, Z. W. Ouyang, *Terahertz Sci. Technol.*, 2012, **5**, 1.
- (20) CCDC No.1505979 contains the crystallographic data deposited at Cambridge Crystallographic Data Center.
- (21) (a) I. D. Brown and D. Altermatt, *Acta Crystallogr.* 1985, **B41**, 244-247. (b) N. E. Brese and M. O'Keeffe, *Acta Crystallogr.* 1991, **B47**, 192-199.
- (22) Y. Zhao, and D. G. Truhlar, *Chem. Phys. Lett.*, 2011, **502**, 1-13.
- (23) Y. Zhao, and D. G. Truhlar, *Theor. Chem. Acc.*, 2008, **120**, 215-241.
- (24) Y. Zhao, and D. G. Truhlar, *Acc. Chem. Res.*, 2008, **41**, 157-167.
- (25) W. J. Hehre, L. Radom, P. R. Schleyer and J. Pople, A. Ab initio Molecular Orbital Theory. Wiley: New York 1986, **100**, 312-312.
- (26) M. J. Frisch, et al. Gaussian 09, (version E.01). (Gaussian, Inc., Wallingford CT), 2010.
- (27) H. Sakiyama, *J. Comput. Chem. Jpn.*, 2007, **6**, 123-134.
- (28) V. Chandrasekhar, A. Dey, A. J. Mota, and E. Colacio.

Journal Name

ARTICLE

- Inorg. Chem., 2013, **52**, 4554–4561.
- (29) M. P. Shores, J. J. Sokol and J. R. Long, *J. Am. Chem. Soc.*, 2002, **124**, 2279-2292.
- (30) Simulations were performed using SPIN developed by Andrew Ozarowski in the National High Magnetic Field Laboratory, USA.
- (31) K. N. Shrivastava, *Phys. Stat. Solidi B.*, 1983, **117**, 437-458.

Magnetically isolated weakly coordinated cobalt(II) ions with unusual electronic structure in mixed-valence metallogrid show field-induced slow magnetization relaxation.

